


Realization of a sign-distinguishable higher-order optical differentiationJunfan Zhu, An Wang, Fuhua Gao,^{*} and Zhiyou Zhang[†]
College of Physics, Sichuan University, Chengdu 610064, China (Received 23 May 2022; accepted 5 August 2022; published 18 August 2022)

A differential operation, which can highlight features of images, is of significant importance in fields such as machine vision. As a front-end action, optical differentiation can overcome the shortcomings of traditional computer differentiation and runs at the speed of light. Compared with the conventional first-order optical differentiation technique, a higher-order one with the correct sign of a differential field obtained can facilitate the recognition of finer features, although relevant studies are relatively scarce. Here, we propose a method to realize sign-distinguishable arbitrary-order optical differentiation by coupling the momentum and polarization of a light field, the feasibility of which is further confirmed by a proof-of-principle experiment. We hope our method will promote the development of optical analog computing, image recognition, and other relevant applications.

DOI: [10.1103/PhysRevA.106.023516](https://doi.org/10.1103/PhysRevA.106.023516)**I. INTRODUCTION**

With the advent and development of computer science, machine vision and computer vision have gradually attracted extensive attention [1–3]. In the era of big data, facial recognition [4], autonomous driving [5], and many other techniques using artificial intelligence are booming. How to quickly filter out the useless from mass information has naturally become a big concern. Traditionally, this task has been accomplished by computer algorithms. However, the ever-increasing amount of data has been slowing down computation speed. Considering that advancement in semiconductor manufacturing is reaching its ceiling, we are obliged to seek other possible solutions.

Differential operations were found to be such an effective method [6]. In a wide variety of applications, machines recognize and classify images by their features. More specifically, features manifest in the intensity variations of these images. A first-order differentiation can highlight areas where the intensity changes dramatically, for instance, the boundaries, and meanwhile can erase the background of a homogeneous light field. If a further step is taken to implement a second-order differentiation, even a uniformly varying light field can be suppressed, and the rate of changes in intensity can be better evaluated. In other words, it can be deemed that with a higher-order differentiation, fine features can be recognized more easily such that image classification can be more convenient and accurate [6,7]. Currently, due to intelligent algorithms and strong computing power, differentiation can be done very well. Nevertheless, it still takes up a certain amount of computing resources. More significantly, computer differentiation deals with the data captured by a detector such as a charge-coupled device (CCD). Therefore, the accuracy of differentiation depends directly on the capability of the detector. Suppose that differentiation is done before detecting;

then not only will the above problems be solved, but it will also be possible to obtain subpixel information. This front-end action should be physical and as fast as possible. Optical differentiation comes into sight.

Optical differentiation, a branch of optical analog computing, aims to realize differentiation using optical elements at the speed of light. It has had a long history of research and has borne fruitful results [8,9]. Recently, being combined with metamaterials [10–17], surface plasmons [18,19], quantum entanglement [20], weak measurement [21], and other fields [22–24], the optical differentiation technique has been further developed. These achievements have enabled optical differentiation to be implemented in modest tabletop laboratory conditions with accessible experimental apparatus.

Moreover, the sign of a differential field is usually not distinguishable due to the fact that we can directly detect only an intensity distribution instead of a field. If the sign can be recovered, more detailed features can be dug out. Efforts have been made to obtain the sign information by introducing a bias light field [25,26]. Benefiting from the precise control system, these methods have great practicability in the first-order differentiation but cannot be plainly generalized to higher-order cases.

In this work, we propose a method of optical differentiation, the fundamental unit of which is a $4f$ system (where f denotes the focal length) with a preselection in the front, a postselection in the rear, and a particular medium placed in the spectrum plane. By cascading the units together and arranging the pre- and postselections inside, a sign-distinguishable arbitrary-order differentiation can be achieved. Furthermore, we experimentally realize a second-order optical differentiation of a Gaussian field to demonstrate the feasibility of our method.

II. OPTICAL DIFFERENTIATION UNIT

The system depicted in Fig. 1 plays the role of a fundamental unit in our method of optical differentiation. Let

^{*}gaofuhua@scu.edu.cn[†]zhangzhiyou@scu.edu.cn

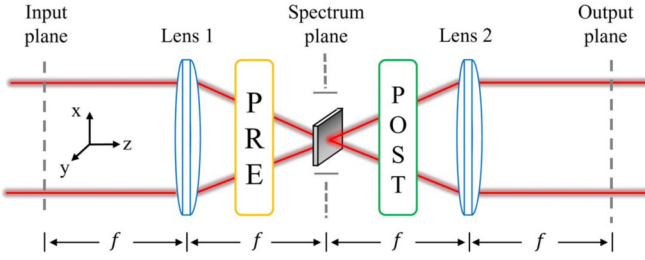


FIG. 1. Schematic diagram of an optical differentiation unit. Lenses 1 and 2 establish the framework of a $4f$ system, where f denotes the focal length. The front-focal plane of lens 1 is the input plane, the back-focal plane of lens 2 is the output plane, and the confocal plane of lenses 1 and 2 is the intermediate plane, also known as the spectrum plane. The plate placed in the spectrum plane gives the anisotropic modulation described in the text. PRE and POST represent the preselection and postselection, respectively.

$|\varphi_0\rangle$ denote the quantum state of photons in the input plane. Hence, the wave function in the position representation is $\varphi_0(x, y) = \langle x, y | \varphi_0 \rangle$, where (x, y) indicates the planar coordinates. The other essential ingredient of optical differentiation is harnessing the polarization. For simplicity, we consider that photons are preselected in the state $|\psi_1\rangle = (|0\rangle + |1\rangle)/\sqrt{2}$, with $|0\rangle$ and $|1\rangle$ denoting the right-handed and left-handed polarization states, or, alternatively, the horizontal and vertical polarization states.

Lens 1 transforms $\varphi_0(x, y)$ to the field $\tilde{\varphi}_0(x_m, y_m)$ in the intermediate plane by

$$\tilde{\varphi}_0(x_m, y_m) = \iint_{-\infty}^{+\infty} \varphi_0(x, y) e^{-i2\pi \frac{xm + ym}{\lambda f}} dx dy, \quad (1)$$

where λ is the wavelength and f is the focal length of lenses 1 and 2. If we make the substitutions $k_x = 2\pi x_m/\lambda f$ and $k_y = 2\pi y_m/\lambda f$, then Eq. (1) can be rewritten as

$$\tilde{\varphi}_0(k_x, k_y) = \iint_{-\infty}^{+\infty} \varphi_0(x, y) e^{-i(k_x x + k_y y)} dx dy := \mathcal{F}\{\varphi_0(x, y)\}, \quad (2)$$

where \mathcal{F} represents the Fourier transform. Indeed, the parameters k_x and k_y characterize a space that is reciprocal to the position space, and therefore, they can be recognized as momenta. Thus, the intermediate plane can also be called the spectrum plane.

Now let us furnish the spectrum plane. We pursue the result that the components of photons in state $|0\rangle$ go through a modulation of $\exp(-i\gamma k_x)$ and, meanwhile, the components in state $|1\rangle$ are modulated by $\exp(i\gamma k_x)$. This result can be achieved by placing a metasurface [12] or a Wollaston-like prism [21] in the spectrum plane. By artificially lithographing local optical axes with different directions on a substance, a Pancharatnam-Berry phase can be generated, and the distinction between the right-handed and left-handed polarization states can be implemented. However, for a Wollaston prism, the eigenstates of polarization should be the horizontal and vertical states instead. It is worth noting that with the spin Hall effect of light, even an isotropic medium is also likely to meet the increased requirement [24]. However, the corresponding mechanism is a bit different.

After the modulation in the spectrum plane, we need to inversely Fourier transform the light field. In practice, the function of lens 2 is also a Fourier transform, which is the same as lens 1. So the difference between a Fourier transform and an inverse Fourier transform will ultimately be reflected in the parity inversion $x \rightarrow -x, y \rightarrow -y$ of the output field. Here, we adopt an inverse Fourier transform to keep the output and input fields directly corresponding. According to the translation property of the Fourier transform, in the output plane the wave functions polarized in states $|0\rangle$ and $|1\rangle$ become $\varphi_0(x - \gamma, y)$ and $\varphi_0(x + \gamma, y)$, respectively.

Suppose that the postselection is made a polarizer that projects photons in the state $|\psi'_1\rangle = (|0\rangle - |1\rangle)/\sqrt{2}$, which is orthogonal to $|\psi_1\rangle$. We obtain the wave function in the output plane, which is given by

$$\begin{aligned} \varphi_1(x, y) &= \frac{\varphi_0(x - \gamma, y) - \varphi_0(x + \gamma, y)}{2} \\ &\approx -\gamma \frac{\partial \varphi_0(x, y)}{\partial x}, \end{aligned} \quad (3)$$

where we have expanded $\varphi_0(x - \gamma, y)$ and $\varphi_0(x + \gamma, y)$ to the second-order term to give the second line. This approximation implies that γ should be sufficiently small or the spatial variation of $\varphi_0(x, y)$ should not be too sharp so that the higher-order terms can be neglected. Equation (3) indicates that a field which takes the form of the partial derivative of $\varphi_0(x, y)$ along with a decay factor γ appears in the output plane.

So far we have elucidated a method to implement a first-order optical differentiation. In order to get a second-order one, an intuitive conjecture is to connect two differentiation units as shown in Fig. 1 together, with the output plane of the first unit being the input plane of the second unit. As a result, the initially prepared state for the second unit is $|\psi_2\rangle = |\psi'_1\rangle$, and therefore, we should choose $|\psi'_2\rangle = (|0\rangle + |1\rangle)/\sqrt{2}$ as the postselected state. It can be readily seen that the wave function in the last output plane reads

$$\begin{aligned} \varphi_2(x, y) &= \frac{\varphi_0(x - 2\gamma, y) + \varphi_0(x + 2\gamma, y) - 2\varphi_0(x, y)}{4} \\ &\approx \gamma^2 \frac{\partial^2 \varphi_0(x, y)}{\partial x^2}, \end{aligned} \quad (4)$$

where $\varphi_0(x - 2\gamma, y)$ and $\varphi_0(x + 2\gamma, y)$ are expanded to the third-order term to yield the second line. The decay factor now is γ^2 . By connecting more differentiation units one by one, we come to the important conclusion that if an n th-order optical differentiation is to be made, then n units are required.

However, the wave function cannot be directly detected. The observable quantity is the probability, which is mathematically equal to the square modulus of the output wave function. As for the first-order differentiation, it is $|\varphi_1(x, y)|^2$, indicating the probability of finding a single photon in the positions labeled by x and y . In practice, since the number of photons used is enormous, we detect the statistical accumulation of $|\varphi_1(x, y)|^2$, namely, the light-intensity distribution. In this way, we cannot tell whether $\partial \varphi_0(x, y)/\partial x$ is positive or negative, so this kind of optical differentiation is incomplete. Knowledge of the sign is necessary in the cases where detailed information about a differential field is required. For example, we are concerned with the change in a local part of

the wave function that should be $\varphi_0(x, y) = -x$. In this way, we cannot tell whether $\varphi_0(x, y)$ is increasing or decreasing as x grows. More discussion about the significance of a sign-distinguishable differentiation is presented in Appendix A.

Another problem exists in that when the phase of the original wave function $\varphi_0(x, y)$ also varies in space, the amplitude and phase information are entangled and then presented in the final light-intensity distribution. For the purpose of realizing a first-order differentiation, we have proposed a method to extract the amplitude and phase separately [21]. However, in the case of higher-order differentiation, the differential fields will be so complicated that separately obtaining the amplitude and phase information becomes hardly possible. To solve this problem, changes in the phase can be suppressed. The most straightforward way is to modulate only the amplitude of a plane wave, which is, nonetheless, too strict. Let us further write the input field as $\varphi_0(x, y) = a(x, y)e^{ib(x, y)}$, where $a(x, y)$ denotes the amplitude and $b(x, y)$ denotes the phase. So the first-order differential field is $\varphi_1 = \left(\frac{\partial a}{\partial x} + ia\frac{\partial b}{\partial x}\right)e^{ib}$. To neglect the phase part, there should be a relation where $\left|\frac{\partial a}{\partial x}\right| \gg a\left|\frac{\partial b}{\partial x}\right|$. We consider a Gaussian beam, which is a typical light source and takes the form

$$G(x, y) = e^{-\frac{x^2+y^2}{w^2(z)}} e^{-i\frac{\pi(x^2+y^2)}{\lambda R(z)}}, \quad (5)$$

where λ is the wavelength and $w(z)$ and $R(z)$ are two z -dependent parameters. The exact expressions of $w(z)$ and $R(z)$ are provided in Ref. [27]. In this case, the above relation is $w^2(z) \ll \lambda R(z)/\pi$. On the other hand, if the amplitude is nearly constant and the phase is small enough, we can approximately have $\varphi_0(x, y) \approx 1 + ib(x, y)$, which thereby indicates that the phase can be considered equivalent to the amplitude in an optical differentiation.

III. SIGN-DISTINGUISHABLE HIGHER-ORDER DIFFERENTIATION

Henceforth, we assume that changes in the phase of $\varphi_0(x, y)$ are relatively small such that only the amplitude

is considered. A measurement scheme will be proposed in which the sign of an arbitrary-order differential field can be recognized and then a complete optical differentiation can be achieved. In order to simplify the calculation, we adopt operator language. The position operator \hat{x} and the momentum operator \hat{k}_x obey the commutation relation $[\hat{x}, \hat{k}_x] = i$, where the reduced Planck constant \hbar has been omitted. In the output plane of the n th differentiation unit, it can be found that

$$\varphi_n(x, y) = \langle x, y | \langle \psi'_n | e^{-i\gamma\hat{\sigma}\hat{k}_x} | \psi_n \rangle | \varphi_{n-1} \rangle, \quad (6)$$

where $\hat{\sigma} = |0\rangle\langle 0| - |1\rangle\langle 1|$. The physical meaning of the unitary operator $e^{-i\gamma\hat{\sigma}\hat{k}_x}$ will be clear if we write it as $e^{-i\gamma\hat{\sigma}\hat{k}_x} = e^{-i\gamma\hat{k}_x}|0\rangle\langle 0| + e^{i\gamma\hat{k}_x}|1\rangle\langle 1|$, with $e^{-i\gamma\hat{k}_x}$ and $e^{i\gamma\hat{k}_x}$ being two displacement operators. So the fields in states $|0\rangle$ and $|1\rangle$ are shifted by a value of γ and $-\gamma$ in the x direction, respectively. Supposing that γ is small enough or the spatial variation of $\varphi_{n-1}(x, y)$ is slow, we can expand $e^{-i\gamma\hat{\sigma}\hat{k}_x}$ and keep it up to the first-order term, namely, $e^{-i\gamma\hat{\sigma}\hat{k}_x} \approx 1 - i\gamma\hat{\sigma}\hat{k}_x$. It follows from Eq. (6) that

$$\begin{aligned} \varphi_n(x, y) &\approx \langle x, y | \langle \psi'_n | (1 - i\gamma\hat{\sigma}\hat{k}_x) | \psi_n \rangle | \varphi_{n-1} \rangle \\ &= \langle \psi'_n | \psi_n \rangle (1 - i\gamma\sigma_n\hat{k}_x) \varphi_{n-1}(x, y) \\ &= \langle \psi'_n | \psi_n \rangle \left(1 - \gamma\sigma_n \frac{\partial}{\partial x}\right) \varphi_{n-1}(x, y), \end{aligned} \quad (7)$$

where $\hat{k}_x|x\rangle = i\frac{\partial}{\partial x}|x\rangle$ is used and σ_n , which is a complex number, is defined as $\sigma_n = \frac{\langle \psi'_n | \hat{\sigma} | \psi_n \rangle}{\langle \psi'_n | \psi_n \rangle}$. It can be noted that σ_n takes a form identical to the weak value in weak-measurement theory [28]. It is also notable that $1 - \gamma\sigma_n\hat{k}_x$ plays the role of the transfer function of our optical differentiation unit. Repeating Eq. (7) n times, the relation between the final output wave function $\varphi_n(x, y)$ and the initial wave function $\varphi_0(x, y)$ can be established, which is given by

$$\begin{aligned} \varphi_n(x, y) &= \langle \psi'_n | \psi_n \rangle \langle \psi'_{n-1} | \psi_{n-1} \rangle \cdots \langle \psi'_1 | \psi_1 \rangle \times \left(1 - \gamma\sigma_n \frac{\partial}{\partial x}\right) \left(1 - \gamma\sigma_{n-1} \frac{\partial}{\partial x}\right) \cdots \left(1 - \gamma\sigma_1 \frac{\partial}{\partial x}\right) \times \varphi_0(x, y) \\ &= \left[1 + \left(\sum_i \sigma_i\right) \left(-\gamma \frac{\partial}{\partial x}\right) + \left(\sum_{i_1 < i_2} \sigma_{i_1} \sigma_{i_2}\right) \left(-\gamma \frac{\partial}{\partial x}\right)^2 + \cdots\right. \\ &\quad \left. + \left(\sum_{i_1 < i_2 < \cdots < i_{n-1}} \sigma_{i_1} \sigma_{i_2} \cdots \sigma_{i_{n-1}}\right) \left(-\gamma \frac{\partial}{\partial x}\right)^{n-1} + \left(\sigma_1 \sigma_2 \cdots \sigma_n\right) \left(-\gamma \frac{\partial}{\partial x}\right)^n\right] \varphi_0(x, y), \end{aligned} \quad (8)$$

where the prefactor $\langle \psi'_n | \psi_n \rangle \cdots \langle \psi'_1 | \psi_1 \rangle$ is neglected since it contains no information about the wave function. Because only the n th-order differential term is to be retained, we must have $\sum_i \sigma_i = 0$, $\sum_{i_1 < i_2} \sigma_{i_1} \sigma_{i_2} = 0, \dots$, $\sum_{i_1 < i_2 < \cdots < i_{n-1}} \sigma_{i_1} \sigma_{i_2} \cdots \sigma_{i_{n-1}} = 0$. Taking σ_1 as the only variable and then solving these equations, it follows that $\sigma_2 \sigma_3 \cdots \sigma_n = (-1)^{n-1} \sigma_1^{n-1}$. Under the circumstances, Eq. (8)

is simplified to

$$\varphi_n(x, y) = \left[1 + (-1)^{n-1} \sigma_1^n \left(-\gamma \frac{\partial}{\partial x}\right)^n\right] \varphi_0(x, y). \quad (9)$$

Equation (9) indicates that the greater the value of $|\sigma_1^n|$ is, the more weight the differential field will carry in $\varphi_n(x, y)$. Thus, according to the formulation of σ_1 , if $\langle \psi'_1 | \psi_1 \rangle$ is close to zero,

a slight change in a differential field can be amplified and then manifested in $\varphi_n(x, y)$.

Suppose that σ_1^n is a real number, and let σ_1^n equal $+\alpha^n$ and $-\alpha^n$, where α is chosen to be real. Recall that only the amplitude is considered, which indicates that $\varphi_0(x, y)$ is real and therefore $\varphi_n(x, y)$ is real. Two fields $\varphi_n^+(x, y)$ and $\varphi_n^-(x, y)$ can be generated, and then two corresponding intensity distributions, say, $\Phi_n^+(x, y) = |\varphi_n^+(x, y)|^2$ and $\Phi_n^-(x, y) = |\varphi_n^-(x, y)|^2$, can be detected. It can be readily found that

$$\Phi_n(x, y) = \Phi_n^+(x, y) - \Phi_n^-(x, y) = -4(\alpha\gamma)^n \frac{\partial^n \varphi_0(x, y)}{\partial x^n}, \quad (10)$$

where the n th-order differential field emerges.

The remaining question is therefore how to gain the two values $\pm\alpha^n$ out of σ_1^n . For the case where n is odd, we can simply make σ_1 be $\pm\alpha$. In practice, this intention can be achieved by setting the two polarization states in $|\psi_1\rangle = (|0\rangle + |1\rangle)/\sqrt{2}$ and $|\psi'_1\rangle = \cos(\frac{\pi}{4} \pm \varepsilon)|0\rangle - \sin(\frac{\pi}{4} \pm \varepsilon)|1\rangle$, respectively. It can be calculated that $\sigma_1 = \mp \cot \varepsilon$. When n is even, the question gets more complicated. σ_1 being two real values apparently cannot satisfy the requirement. Thus, we take full advantage of the fact that σ_1 is a complex value and write it as $\sigma_1 = u + iv$. Then we solve the two equations $\text{Re}\{(u + iv)^n\} = \pm\alpha^n$ and $\text{Im}\{(u + iv)^n\} = 0$. For example, if $n = 2$, we can have the possible solution $\sigma_1 = \alpha, i\alpha$. If $n = 4$, the two equations may yield two valid solutions, $\sigma_1 = \alpha, (\alpha + i\alpha)/\sqrt{2}$. As we want to practically get a complex σ_1 , the two polarization states can be chosen to be $|\psi_1\rangle = (|0\rangle + |1\rangle)/\sqrt{2}$ and $|\psi'_1\rangle = e^{i\theta} \cos(\frac{\pi}{4} + \varepsilon)|0\rangle - e^{-i\theta} \sin(\frac{\pi}{4} + \varepsilon)|1\rangle$. Assuming that $\theta, \varepsilon \ll 1$, we have $\sigma_1 \approx -\frac{\varepsilon - i\theta}{\varepsilon^2 + \theta^2}$. With suitable selections of θ and ε , the required σ_1 can be generated.

IV. PROOF-OF-PRINCIPLE EXPERIMENT

In the following, we use a proof-of-principle experiment to confirm the feasibility of our method, in which the second-order differentiation of a Gaussian beam $G(x, y)$ with a wavelength of 633 nm is implemented. Two differentiation units are required. Since the size of a Gaussian laser increases with propagation and the relation $w^2(z) \ll \lambda R(z)/\pi$ must hold, we make the distance between the two lenses of each unit slightly longer than $2f$, such that the laser spot can be shrunk. A Wollaston prism is placed in the spectrum plane. Thus, the ground state $|0\rangle$ and $|1\rangle$ should respectively be the horizontal state, say, $|H\rangle$, and the vertical state, say, $|V\rangle$. The value of γ depends mainly on the length-width ratio of the Wollaston prism and the focal length of the lenses. To clearly understand how an optical differentiation can be achieved by a Wollaston prism, readers may refer to Appendix C. In our experiment, γ is about $10 \mu\text{m}$. Let the preselection of the first unit be a polarizer (P1) with its axis lying at an angle of $\pi/4$ such that the preselected state is $|\psi_1\rangle = (|H\rangle + |V\rangle)/\sqrt{2}$. If the postselection in the first unit is another polarizer (P2) that is orthogonal to the first one, which gives $\sigma_1 \rightarrow \infty$, then we arrive at the result same as in Eq. (3). Since the postselection of the first unit can simply be the preselection of the second unit, henceforth, we take into account only the postselection in the second unit. If this postselection is also a polarizer (P3)

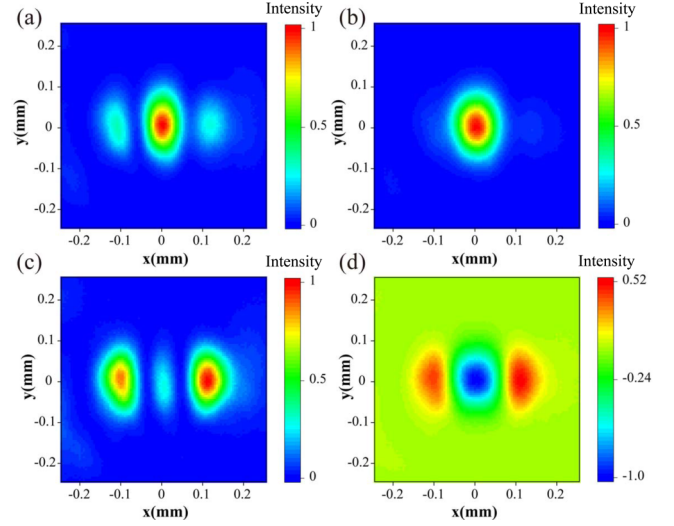


FIG. 2. Light-intensity distributions when (a) $\sigma_1 \rightarrow \infty$, (b) $\sigma_1 = \alpha$, and (c) $\sigma_1 = i\alpha$. (d) The second-order differential field of a Gaussian beam. All distributions are normalized.

whose axis is orthogonal to that of P2, we arrive at Eq. (4), and the corresponding intensity distribution that is detected by a CCD is shown in Fig. 2(a). It can be seen that there are three peaks. The middle peak is the highest. The left and right peaks with nearly the same height are symmetrically distributed with respect to the middle one. In the following, we will obtain the second-order differential field by respectively setting $\sigma_1 = \alpha$ and $i\alpha$.

First, we consider $\sigma_1 = \alpha$. Because σ_1 is real, the postselection in the first unit can also simply be a polarizer, namely, P2, with its axis lying at $\varepsilon - \pi/4$ such that $|\psi'_1\rangle = \cos(\frac{\pi}{4} - \varepsilon)|H\rangle - \sin(\frac{\pi}{4} - \varepsilon)|V\rangle$. It follows that $\sigma_1 = \cot \varepsilon = \alpha$. Recalling that the relation $\sigma_1 + \sigma_2 = 0$ should hold, we rotate P3 to a particular angle in which $\sigma_2 = -\sigma_1$. Since any two successive polarization states are no longer orthogonal to each other, the total intensity of the field increases with the increase of the prefactor $\langle \psi_2 | \psi_2 \rangle \langle \psi'_1 | \psi_1 \rangle$ in Eq. (8), or, more specifically, with the increase of ε . However, we are not concerned about the growth of the total intensity, so the prefactors are disregarded, and intensity distributions are normalized. In this case, it seems that the height of the middle peak increases while the heights of the two side peaks decrease, which leads to the distribution shown in Fig. 2(b). Second, let us consider the case where $\sigma_1 = i\alpha$. We reset every two successive polarizers to the mutually orthogonal polarization states. When σ_1 is purely imaginary, we can place a quarter-wave plate (QWP) before P2, and then the QWP and P2 together constitute the postselection. The fast axis of QWP is parallel to the polarization direction of P2. When P2 is rotated by an angle of $-\theta$, the postselected state becomes $|\psi'_1\rangle = (e^{i\theta}|H\rangle - e^{-i\theta}|V\rangle)/\sqrt{2}$ (see Appendix B). So it follows that $\sigma_1 = i \cot \theta = i\alpha$. It is important to note that for this case the preselected state in the second unit is not $|\psi'_1\rangle$, but $|\psi_2\rangle = \cos(\frac{\pi}{4} + \theta)|H\rangle - \sin(\frac{\pi}{4} + \theta)|V\rangle$. To simplify the question, we rotate the coordinate system of the second unit by an angle of $-\theta$ such that $|\psi_2\rangle = (|H\rangle - |V\rangle)/\sqrt{2}$, and meanwhile, the axis of P3 will change to $\pi/4 + \theta$, indicating

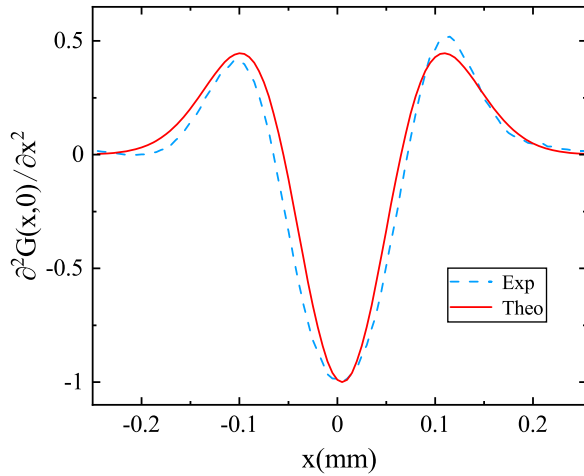


FIG. 3. The cross-section distribution of the second-order differential field of a Gaussian beam. The red solid curve and the blue dashed curve correspond to the theoretical and experimental results, respectively.

a rotation angle of θ . After we insert another QWP before P3 with its fast axis pointing at $\pi/4$, it can be calculated that $\sigma_2 = -i \cot \theta = -\sigma_1$. With θ increasing, the height of the middle peak shrinks, but the two symmetric peaks grow, which is just the inverse of the case of a real σ_1 . By making θ equal to ε , we show the resultant distribution in Fig. 2(c).

The last step is to subtract the distribution of $\sigma_1 = \alpha$ from that of $\sigma_1 = i\alpha$, as indicated by Eq. (10). Due to the limitation of experimental conditions, we cannot get the absolute values of light intensities. Nonetheless, through numerical simulation, we found that when the maximum intensity of $\sigma_1 = \alpha$ was nearly twice as strong as that of $\sigma_1 = i\alpha$, the experimental result of the cross-section distribution $\partial^2 G(x, 0)/\partial x^2$ agreed well with the theoretical expectation, as presented in Fig. 3. The slight deviation of the theoretical and experimental curves in the middle peak may result from the imperfection of the laser source and the diffraction effects in the propagation of light. The unequal heights of the two small peaks may be attributed to the artificial error when polarizers and wave plates were not precisely rotated. So eventually, we can plot the second-order differential field in Fig. 2(d), where two relatively small peaks have positive heights and the highest peak located in the middle is negative.

V. DISCUSSION AND CONCLUSION

The question of the efficiency of this optical differentiation method arises. Reconsider the prefactor $\langle \psi'_n | \psi_n \rangle \cdots \langle \psi'_1 | \psi_1 \rangle$ and input it into Eq. (10). If every successive pre- and postselection is nearly orthogonal, $\Phi_n(x, y)$ will be approximately proportional to γ^n , which implies that we have to obtain the n th-order differential field at the cost of γ^n attenuation of the light intensity. Fortunately, detecting an overly high-order differential field is not of great significance in practice. In addition, the optical elements that we used, such as lenses, will introduce aberrations, so the overly high-order differential setup will be difficult to put to good use due to systematic error. External perturbation can also worsen the signal-to-noise

ratio. On the other hand, one may worry that two measurements will be so time-consuming that rapid detection cannot be achieved. This problem can be solved by a beam splitter that can split $\varphi_0(x, y)$ into two paths. In this way, $\Phi_n^+(x, y)$ and $\Phi_n^-(x, y)$ can be separately and simultaneously obtained.

Methods to miniaturize systems are also an important topic for optical analog computing. The $4f$ systems, which can modulate the light field and constrain the diffraction effect, are essential in optical systems that have a rather long length, such as telescopes and microscopes. However, for a miniaturized integrated optical system such as a cell phone camera, the $4f$ setup may be bulky. It is very likely that the $4f$ system in the differentiation unit could be replaced by an ultrathin birefringent crystal or a particularly designed metamaterial in the future.

In conclusion, we have elaborated an optical differentiation unit which is based on a $4f$ system. By connecting such n units one by one, an n th-order optical differentiation setup can be established. Since it is hardly possible to separately extract the amplitude and the phase from a high-order differential field, we have paid attention to applications where the differentiation of the phase can be ignored. Through particular settings for the pre- and postselections, only the nondifferential and n th-order differential terms can be retained, and thereafter, a sign-distinguishable differential field can be obtained by subtraction of two intensity distributions. We have also implemented a proof-of-principle experiment. The resultant distribution that contains three peaks is basically consistent with the characteristics of the second-order differential field of a Gaussian beam, confirming the validity of our method. Despite some technical difficulties such as the elimination of aberrations and the miniaturization of the setup, we believe this method of optical differentiation will be of great use in optical analog computing, machine vision, and many other applications.

ACKNOWLEDGMENT

This work is supported by the Natural Science Foundation of China (Grant No. 11674234) and the Science Specialty Program of Sichuan University (Grant No. 2020SCUNL210).

APPENDIX A: SIGNIFICANCE OF A SIGN-DISTINGUISHABLE OPTICAL DIFFERENTIATION

Conventional applications of optical differentiation are mostly about edge detection. For edge detection, only the magnitude of a differential field matters, which means that the sign distinguishability is unnecessary. Therefore, we will table some cases other than edge detection to show the significance of sign-distinguishable optical differentiation in this Appendix.

As shown in the differentiation unit, when we place the working axis of the modulator along the x axis in the spectrum plane, we can realize a differentiation with respect to x . Now suppose we want to realize a differentiation with respect to an arbitrary direction; then we have to rotate the working axis to the right direction, which is time-consuming and can introduce experimental error. Alternatively, we can respectively measure $\partial\varphi(x, y)/\partial x$ and $\partial\varphi(x, y)/\partial y$, where $\varphi(x, y)$

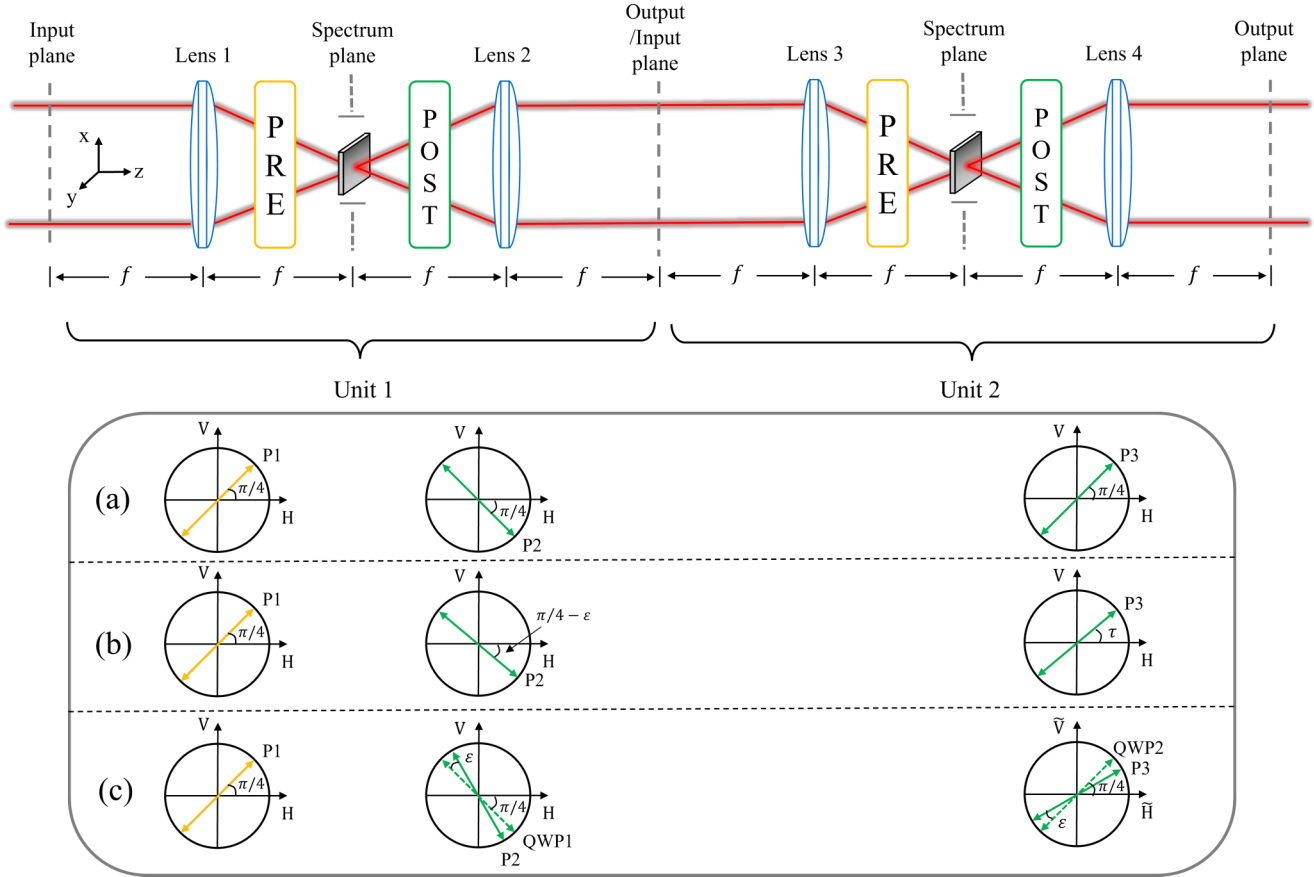


FIG. 4. The top part presents the experimental setup of a second-order optical differentiation, which is obtained by docking two differentiation units together. The bottom part indicates the pre- and postselections inside. The settings of blocks (a), (b), and (c) correspond to the results shown in Figs. 2(a)–2(c), respectively.

is the field to be differentiated. Then it is possible to use the relation $\frac{\partial \varphi(x,y)}{\partial s} = \cos \theta \frac{\partial \varphi(x,y)}{\partial x} + \sin \theta \frac{\partial \varphi(x,y)}{\partial y}$ to obtain the directional differential field with respect to an arbitrary angle θ . This way of obtaining $\partial \varphi(x,y)/\partial s$ certainly requires knowledge of the signs of $\partial \varphi(x,y)/\partial x$ and $\partial \varphi(x,y)/\partial y$. An interesting application derived from this method is identifying the direction of motion. A snapshot of a moving object could be blurry. The absolute value of its differential field reduces to the minimum in the exact motion direction. Therefore, a powerful identification method is just to find the angle where $\int |\frac{\partial \varphi(x,y)}{\partial s}| dx dy$ is minimized. In our recent work, we experimentally demonstrated it [29].

A sign-distinguishable optical differentiation can also be utilized to reconstruct wave functions. Let us write a wave function as $\varphi(x) = a(x)e^{ib(x)}$. To obtain the wave function we first measure $da(x)/dx$ and $db(x)/dx$ and then use an integral algorithm, e.g., the Fourier integral algorithm [21,26] and the Hudgin algorithm [30], to recover $a(x)$ and $b(x)$. For any kind of algorithm, knowledge of the signs of $da(x)/dx$ and $db(x)/dx$ is necessary. This method can be of great importance in wave-front sensing.

In image recognition, the sign of a differential field also contains information. Suppose a light beam is reflected by a slab which is composed of several kinds of materials. Due to the differences of different materials in reflectivity and roughness, the amplitude of the reflected light will no longer

be constant but will carry information about the distribution of different materials. For the case where the sign of a differential field is unknown, we can identify only where the kind of material changes. If the sign is known, then it becomes possible to further ascertain the kinds of materials in different regions. Moreover, we can consider that the transition area is not narrow, so the amplitude of the reflected light can be smoothly and slowly changed, in which case higher-order differentiation can be useful.

To sum up, the sign distinguishability can be critical in some application scenarios.

APPENDIX B: DETAILS OF THE EXPERIMENT

We provide more details about how we obtained Fig. 2 in the main text to help readers better understand the experiment.

First, we show how to obtain Fig. 2(a). To realize a second-order optical differentiation, we cascade two differentiation units together to give the setup shown in Fig. 4. Let us write the wave function in the leftmost input plane as $\varphi_0(x,y)$. The three circles in block (a) indicate the setting of the pre- and postselections. The preselection of unit 1 is a polarizer (P1) with its axis pointing at $\pi/4$, which means the preselected state is

$$|\psi_1\rangle = \frac{1}{\sqrt{2}}(|H\rangle + |V\rangle). \quad (B1)$$

The postselection of unit 1 is another polarizer (P2) with its axis pointing at $-\pi/4$. So the postselected state is

$$|\psi'_1\rangle = \frac{1}{\sqrt{2}}(|H\rangle - |V\rangle). \quad (\text{B2})$$

According to Eq. (7), the wave function in the output plane of unit 1 is given by

$$\begin{aligned} \varphi_1(x, y) &= \langle x, y | \langle \psi'_1 | (1 - i\gamma \hat{\sigma} \hat{k}_x) | \psi_1 \rangle | \varphi_0 \rangle \\ &= \langle x, y | (-i\gamma \hat{k}_x) | \varphi_0 \rangle \\ &= -\gamma \frac{\partial}{\partial x} \varphi_0(x, y), \end{aligned} \quad (\text{B3})$$

where $\hat{\sigma} = |H\rangle\langle H| - |V\rangle\langle V|$. Since the postselection of unit 1 can be directly utilized as the preselection of unit 2, the preselection of unit 2 can simply be none, and therefore, the preselected state of unit 2 is $|\psi_2\rangle = |\psi'_1\rangle$. We set the postselection of unit 2 to be a polarizer (P3) whose axis lies at $\pi/4$, and then the postselected state of unit 2 is

$$|\psi'_2\rangle = \frac{1}{\sqrt{2}}(|H\rangle + |V\rangle). \quad (\text{B4})$$

In a similar manner, the wave function in the output plane of unit 2 is given by

$$\begin{aligned} \varphi_2(x, y) &= \langle x, y | \langle \psi'_2 | (1 - i\gamma \hat{\sigma} \hat{k}_x) | \psi_2 \rangle | \varphi_1 \rangle \\ &= \langle x, y | (-i\gamma \hat{k}_x) | \varphi_1 \rangle \\ &= -\gamma \frac{\partial}{\partial x} \varphi_1(x, y) \\ &= \gamma^2 \frac{\partial^2}{\partial x^2} \varphi_0(x, y). \end{aligned} \quad (\text{B5})$$

For the case where a Gaussian beam is considered as the initial input, it leads to $\varphi_0(x, y) = G(x, y)$. We finally obtain the intensity distribution, which is presented in Fig. 2(a).

Next, we manage to obtain the intensity distribution shown in Fig. 2(b). In this case, we choose the experimental settings depicted in block (b). The preselection of unit 1 is still a polarizer (P1) with its axis set at $\pi/4$, and therefore, the preselected state remains the same. However, the second polarizer (P2) as the postselection of unit 1 is rotated by an angle of ε , which yields the postselected state

$$|\psi'_1\rangle = \cos\left(\frac{\pi}{4} - \varepsilon\right)|H\rangle - \sin\left(\frac{\pi}{4} - \varepsilon\right)|V\rangle. \quad (\text{B6})$$

Now the wave function in the output plane of unit 1 is given by

$$\begin{aligned} \varphi_1(x, y) &= \langle x, y | \langle \psi'_1 | (1 - i\gamma \hat{\sigma} \hat{k}_x) | \psi_1 \rangle | \varphi_0 \rangle \\ &= \left(1 - \gamma \cot \varepsilon \frac{\partial}{\partial x}\right) \varphi_0(x, y), \end{aligned} \quad (\text{B7})$$

where the prefactor $\langle \psi'_1 | \psi_1 \rangle$ has been neglected. The preselected state of unit 2 takes the form of the postselected state of unit 1, say, $|\psi_2\rangle = |\psi'_1\rangle$. The axis of the polarizer (P3) which plays the role of the postselection in unit 2 should be chosen at a particular angle τ such that

$$|\psi'_2\rangle = \cos \tau |H\rangle + \sin \tau |V\rangle \quad (\text{B8})$$

and the relation $\sigma_2 = -\cot \varepsilon = -\sigma_1$ is satisfied. Therefore, the field in the output plane is

$$\begin{aligned} \varphi_2^+(x, y) &= \langle x, y | \langle \psi'_2 | (1 - i\gamma \hat{\sigma} \hat{k}_x) | \psi_2 \rangle | \varphi_1 \rangle \\ &= \langle x, y | [1 - i\gamma(\sigma_1 + \sigma_2)\hat{k}_x - \gamma^2 \sigma_1 \sigma_2 \hat{k}_x^2] | \varphi_0 \rangle \\ &= \left(1 - \gamma^2 \cot^2 \varepsilon \frac{\partial^2}{\partial x^2}\right) \varphi_0(x, y), \end{aligned} \quad (\text{B9})$$

where the prefactor $\langle \psi'_2 | \psi_2 \rangle$ has also been neglected. Figure 2(b) shows the intensity distribution $\Phi_2^+(x, y) = |\varphi_2^+(x, y)|^2$.

The principle of getting Fig. 2(c) is the same as that of getting Fig. 2(b). However, this time an imaginary σ_1 is to be generated. Therefore, a quarter-wave plate (QWP1) with its fast axis placed at $-\pi/4$ is inserted before (or to the left of) the second polarizer (P2), as shown in block (c). QWP1 and P2 together constitute the postselection of unit 1. With $|H\rangle$ and $|V\rangle$ being the eigenvectors, the action of QWP1 can be represented by the matrix $\frac{1}{\sqrt{2}} \begin{bmatrix} 1 & -i \\ -i & 1 \end{bmatrix}$. So the postselected state reads

$$\begin{aligned} |\psi'_1\rangle &= \frac{1}{\sqrt{2}} \begin{bmatrix} 1 & -i \\ -i & 1 \end{bmatrix} \begin{bmatrix} \cos(\frac{\pi}{4} + \varepsilon) \\ -\sin(\frac{\pi}{4} + \varepsilon) \end{bmatrix} \\ &= \frac{1}{\sqrt{2}} e^{i\pi/4} \begin{bmatrix} e^{i\varepsilon} \\ -e^{-i\varepsilon} \end{bmatrix} \\ &\equiv \frac{1}{\sqrt{2}} (e^{i\varepsilon} |H\rangle - e^{-i\varepsilon} |V\rangle), \end{aligned} \quad (\text{B10})$$

where in the third line the phase term $e^{i\pi/4}$ has been discarded since it does not contribute to the intensity distribution. It follows that $\sigma_1 = i \cot \varepsilon$. The remaining problem is how to construct $\sigma_2 = -\sigma_1$. We must note that since P2 is the last element in the postselection of unit 1, here, the preselected state of unit 2 is no longer just the postselected state of unit 1. Instead, it is solely decided by P2, i.e., $|\psi_2\rangle = \cos(\frac{\pi}{4} + \varepsilon)|H\rangle - \sin(\frac{\pi}{4} + \varepsilon)|V\rangle$. Note that σ_2 should also be imaginary, so another combination of a quarter-wave plate (QWP2) and a polarizer (P3) is set as the postselection of unit 2. If we rotate the coordinate system of unit 2 by an angle $-\varepsilon$, then the preselected state becomes $|\psi_2\rangle = \frac{1}{\sqrt{2}}(|\tilde{H}\rangle - |\tilde{V}\rangle)$. In the new coordinate system, the fast axis of QWP2 is placed at $\pi/4$, and the axis of P3 is placed at $\pi/4 - \varepsilon$. The postselected state is then given by

$$\begin{aligned} |\psi'_2\rangle &= \frac{1}{\sqrt{2}} \begin{bmatrix} 1 & i \\ i & 1 \end{bmatrix} \begin{bmatrix} \cos(\frac{\pi}{4} - \varepsilon) \\ \sin(\frac{\pi}{4} - \varepsilon) \end{bmatrix} \\ &= \frac{1}{\sqrt{2}} e^{i\pi/4} \begin{bmatrix} e^{-i\varepsilon} \\ e^{i\varepsilon} \end{bmatrix} \\ &\equiv \frac{1}{\sqrt{2}} (e^{-i\varepsilon} |\tilde{H}\rangle + e^{i\varepsilon} |\tilde{V}\rangle). \end{aligned} \quad (\text{B11})$$

We have $\sigma_2 = -i \cot \varepsilon = -\sigma_1$. In the output plane, the wave function is given by

$$\varphi_2^-(x, y) = \left(1 + \gamma^2 \cot^2 \varepsilon \frac{\partial^2}{\partial x^2}\right) \varphi_0(x, y). \quad (\text{B12})$$

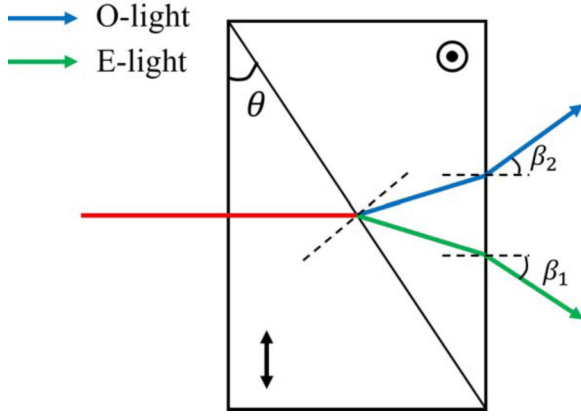


FIG. 5. Function diagram of the Wollaston prism.

We can experimentally detect the intensity distribution $\Phi_2^-(x, y) = |\varphi_2^-(x, y)|^2$, which is shown in Fig. 2(c).

APPENDIX C: WOLLASTON PRISM

In this Appendix, we give a more detailed description of the Wollaston prism, which is used as a modulator in the spectrum plane of our differentiation unit.

A function diagram of the Wollaston prism is shown in Fig. 5. Let n_o and n_e denote the refractive indices of the so-called ordinary light (O-light) and extraordinary light (E-light). O-light and E-light correspond to the horizontal polarization state $|H\rangle$ and vertical polarization state $|V\rangle$, respectively. Through straightforward calculation, it can be found that

$$\beta_1 \approx \beta_2 \approx \arcsin[\tan \theta (n_o - n_e)] \equiv \beta. \quad (C1)$$

Let the input field be $\varphi_0(x, y)$. Then in the spectrum plane where the Wollaston prism is placed, the Fourier-transformed field is given by

$$\tilde{\varphi}_0(x_m, y_m) = \iint_{-\infty}^{+\infty} \varphi_0(x, y) e^{-i2\pi \frac{x_m x + y_m y}{\lambda f}} dx dy, \quad (C2)$$

where λ is the wavelength and f is the focal length of lens. As can be seen in Fig. 5, O-light is rotated by an angle of β , and E-light is rotated by $-\beta$, which means the corresponding fields can be mathematically expressed as $\tilde{\varphi}_0(x_m, y_m) e^{-i2\pi \frac{x_m \sin \beta}{\lambda}} |H\rangle$ and $\tilde{\varphi}_0(x_m, y_m) e^{i2\pi \frac{x_m \sin \beta}{\lambda}} |V\rangle$. By making inverse Fourier transforms, it follows that

$$\begin{aligned} \varphi_1(x, y) |H\rangle &= \iint_{-\infty}^{+\infty} \tilde{\varphi}_0(x_m, y_m) e^{-i2\pi \frac{x_m \sin \beta}{\lambda}} e^{i2\pi \frac{x_m x + y_m y}{\lambda f}} |H\rangle dx_m dy_m \\ &= \iint_{-\infty}^{+\infty} \tilde{\varphi}_0(x_m, y_m) e^{i2\pi \frac{x_m(x - f \sin \beta) + y_m y}{\lambda f}} |H\rangle dx_m dy_m \\ &= \varphi_0(x - f \sin \beta, y) |H\rangle \end{aligned} \quad (C3)$$

and

$$\begin{aligned} \varphi_1(x, y) |V\rangle &= \iint_{-\infty}^{+\infty} \tilde{\varphi}_0(x_m, y_m) e^{i2\pi \frac{x_m \sin \beta}{\lambda}} e^{i2\pi \frac{x_m x + y_m y}{\lambda f}} |V\rangle dx_m dy_m \\ &= \iint_{-\infty}^{+\infty} \tilde{\varphi}_0(x_m, y_m) e^{i2\pi \frac{x_m(x + f \sin \beta) + y_m y}{\lambda f}} |V\rangle dx_m dy_m \\ &= \varphi_0(x + f \sin \beta, y) |V\rangle. \end{aligned} \quad (C4)$$

Therefore, it can be found that $\gamma = f \sin \beta$, which indicates that we can change the value of γ by changing the length-width ratio θ or the focal length f .

-
- [1] S. Kurada and C. Bradley, *Comput. Ind.* **34**, 55 (1997).
 - [2] L. Pérez, R. Íñigo, N. Rodríguez, R. Usamentiaga, and D. F. García, *Sensors* **16**, 335 (2016).
 - [3] P. Vithu and J. Moses, *Trends Food Sci. Technol.* **56**, 13 (2016).
 - [4] M. Loey, G. Manogaran, M. H. N. Taha, and N. E. M. Khalifa, *Measurement (London)* **167**, 108288 (2021).
 - [5] Y. Cai, T. Luan, H. Gao, H. Wang, L. Chen, Y. Li, M. A. Sotelo, and Z. Li, *IEEE Trans. Instrum. Meas.* **70**, 1 (2021).
 - [6] R. Jain, R. Kasturi, and B. G. Schunck, *Machine Vision* (McGraw-Hill, New York, 1995), Vol. 5.
 - [7] B. Zhang, Y. Gao, S. Zhao, and J. Liu, *IEEE Trans. Image Process.* **19**, 533 (2010).
 - [8] S. K. Yao and S. H. Lee, *J. Opt. Soc. Am.* **61**, 474 (1971).
 - [9] C. Preza, D. L. Snyder, and J.-A. Conchello, *J. Opt. Soc. Am. A* **16**, 2185 (1999).
 - [10] A. Silva, F. Monticone, G. Castaldi, V. Galdi, A. Alù, and N. Engheta, *Science* **343**, 160 (2014).
 - [11] Q. He, F. Zhang, M. Pu, X. Ma, X. Li, J. Jin, Y. Guo, and X. Luo, *Nanophotonics* **10**, 741 (2021).
 - [12] J. Zhou, S. Liu, H. Qian, Y. Li, H. Luo, S. Wen, Z. Zhou, G. Guo, B. Shi, and Z. Liu, *Sci. Adv.* **6**, eabc4385 (2020).
 - [13] J. Zhou, H. Qian, J. Zhao, M. Tang, Q. Wu, M. Lei, H. Luo, S. Wen, S. Chen, and Z. Liu, *Natl. Sci. Rev.* **8**, nwaa176 (2020).
 - [14] H. Wang, C. Guo, Z. Zhao, and S. Fan, *ACS Photon.* **7**, 338 (2020).

- [15] Y. Zhou, H. Zheng, I. I. Kravchenko, and J. Valentine, *Nat. Photon.* **14**, 316 (2020).
- [16] C. Guo, M. Xiao, M. Minkov, Y. Shi, and S. Fan, *Optica* **5**, 251 (2018).
- [17] J. Sol, D. R. Smith, and P. del Hougne, *Nat. Commun.* **13**, 1713 (2022).
- [18] T. Zhu, Y. Zhou, Y. Lou, H. Ye, M. Qiu, Z. Ruan, and S. Fan, *Nat. Commun.* **8**, 15391 (2017).
- [19] T.-J. Huang, J. Zhao, L.-Z. Yin, and P.-K. Liu, *Opt. Lett.* **46**, 2746 (2021).
- [20] J. Liu, Q. Yang, S. Chen, Z. Xiao, S. Wen, and H. Luo, *Phys. Rev. Lett.* **128**, 193601 (2022).
- [21] J. Zhu, A. Wang, X. Liu, Y. Liu, Z. Zhang, and F. Gao, *Phys. Rev. A* **104**, 032221 (2021).
- [22] W. Xu, X. Ling, D. Xu, S. Chen, S. Wen, and H. Luo, *Phys. Rev. A* **104**, 053513 (2021).
- [23] D. Xu, S. He, J. Zhou, S. Chen, S. Wen, and H. Luo, *Opt. Lett.* **45**, 6867 (2020).
- [24] T. Zhu, Y. Lou, Y. Zhou, J. Zhang, J. Huang, Y. Li, H. Luo, S. Wen, S. Zhu, Q. Gong, M. Qiu, and Z. Ruan, *Phys. Rev. Appl.* **11**, 034043 (2019).
- [25] D. Gorlitz and F. Lenz, *J. Opt.* **8**, 289 (1977).
- [26] T. Zhu, J. Huang, and Z. Ruan, *Adv. Photon.* **2**, 016001 (2020).
- [27] W. Nagourney, *Quantum Electronics for Atomic Physics and Telecommunication* (Oxford University Press, Oxford, 2014).
- [28] Y. Aharonov, D. Z. Albert, and L. Vaidman, *Phys. Rev. Lett.* **60**, 1351 (1988).
- [29] A. Wang, J. Zhu, L. Luo, X. Liu, L. Ye, Z. Zhang, and J. Du, *Opt. Lett.* **47**, 3880 (2022).
- [30] M. Yang, Y. Xiao, Y.-W. Liao, Z.-H. Liu, X.-Y. Xu, J.-S. Xu, C.-F. Li, and G.-C. Guo, *Laser Photon. Rev.* **14**, 1900251 (2020).